International Journal of Thermophysics (2020) 41:97
https://doi.org/10.1007/s10765-020-02670-3

Wave Propagation in Two-Temperature Porothermoelasticity

Baljeet Singh[1]

Received: 22 March 2020 / Accepted: 19 April 2020

Abstract
In the present paper, the governing equations for two-temperature generalized porothermoelasticity are formulated in accordance with Green and Naghdi theory of thermoelasticity without energy dissipation. Two-dimensional plane wave solution of these governing equations indicates the existence of one shear vertical and four coupled longitudinal waves in porothermoelastic medium. A problem on reflection of longitudinal and shear waves is considered at a thermally insulated and stress-free surface of a generalized porothermoelastic solid half-space. The appropriate potentials for incident and reflected waves satisfy the required boundary conditions at free surface of the half-space and a non-homogeneous system of five equations in reflection coefficients is obtained. The expressions for energy ratios of reflected waves are obtained for incidence of both longitudinal and shear waves. The numerical results are obtained for values of porosity lying between 0.01 and 0.5, which are suitable for most of rocks present in the earth's crust. The experimental data of kerosene-saturated sandstone are selected for numerical computations to observe the effects of two-temperature parameters and porosity on the energy ratios of reflected waves.

Keywords Energy ratios · Green–Naghdi theory · Plane waves · Porothermoelasticity · Reflection · Two-temperature

1 Introduction

Biot [1] developed the theory of poroelasticity, which has been applied in most investigations on wave propagation in fluid-saturated rocks. Biot [2, 3] analyzed the isothermal wave propagation in fluid-saturated elastic porous media for both high and low frequency ranges. He showed the existence of two longitudinal waves and one shear wave, which are dispersive and dissipative. Thereafter, many

✉ Baljeet Singh
bsinghgc11@gmail.com

[1] Department of Mathematics, Post Graduate Government College Sector 11, Chandigarh 160011, India

Published online: 13 May 2020

research workers including [4–30] contributed toward wave propagation phenomena in poroelasticity. Some problems on numerical simulations in porous media were attempted [31–34].

Wave propagation problems in saturated thermoelastic porous medium have many applications in various engineering fields including petroleum engineering, chemical engineering, pavement engineering and nuclear waste management. Biot [35] formulated the general laws of thermoelasticity and principle of minimum entropy production. These laws and principle proved a basis for many researches in saturated thermoelastic porous medium [36–55].

Chen and Gurtin [56] and Chen et al. [57, 58] developed a coupled linear theory of thermoelasticity involving the conductive and thermodynamic temperatures. This two-temperature theory of thermoelasticity reduces to classical theory of thermoelasticity when the conductive temperature equals to the thermodynamic temperature. Using this two-temperature theory, Warren and Chen [59] and Puri and Jordan [60] investigated the wave propagation problems to examine several measures of wave fields. Youssef [61, 62] developed theories of two-temperature thermoelasticity in context of Lord and Shulman [63] and Green and Naghdi [64] models. In context of these theories, various wave propagation problems were investigated by many researchers [65–69].

In contrast to the classical thermoelasticity associated with Fourier's law of heat conduction, the main feature of Green and Naghdi [64] theory is that the heat flow does not involve energy dissipation. Youssef [45] developed the governing equations of thermoelastic porous medium in the context of Lord-Shulman [63] theory of generalized thermoelasticity with one relaxation time. The main objective of this paper is to formulate a two-temperature porothermoelasticity without energy dissipation. In Sect. 2, a set of governing equations of two-temperature thermoelasticity of porous medium without energy dissipation is developed in context of theories proposed by Youssef [45, 62] and Green and Naghdi [64]. In Sect. 3, the governing equations are specialized in (x, y) plane and solved for plane waves. It is shown that there exist one shear vertical and four longitudinal waves in a two-dimensional porothermoelastic solid half-space. In Sects. 4 and 5, a reflection phenomenon of plane waves is studied at a thermally insulated and stress-free surface of a half-space. The relations between reflection coefficients and the analytical expressions for energy ratios are obtained. In Sect. 6, the numerical computations are carried out for rock materials having porosity between 0.01 and 0.5. The experimental data of kerosene-saturated sandstone are used to graphically illustrate the dependence of energy ratios of reflected waves on two-temperature parameters and porosity. The theoretical and numerical results are summarized in the last section.

2 Governing Equations

In context of theories proposed by Green and Naghdi [64] and Youssef [45, 62], the governing equations of a linear, homogeneous and isotropic two-temperature generalized porothermoelasticity without energy dissipation in the absence of body forces and heat sources, can be expressed as

(a) Constitutive equations

$$e_{ij} = \frac{1}{2}\left(\frac{\partial u_i}{\partial x_j} + \frac{\partial u_j}{\partial x_i}\right), \qquad \epsilon = \frac{\partial U_i}{\partial x_i}, \tag{1}$$

$$\sigma_{ij} = 2\mu e_{ij} + (\lambda e_{kk} + Q\epsilon - R_{11}\Theta^s - R_{12}\Theta^f)\delta_{ij}, \tag{2}$$

$$\sigma = Qe_{kk} + R\epsilon - R_{21}\Theta^s - R_{22}\Theta^f, \tag{3}$$

(b) Equations of motion

$$\mu\frac{\partial^2 u_i}{\partial x_j^2} + (\lambda+\mu)\frac{\partial^2 u_j}{\partial x_i \partial x_j} + Q\frac{\partial^2 U_j}{\partial x_i \partial x_j} - R_{11}\frac{\partial \Theta^s}{\partial x_i} - R_{12}\frac{\partial \Theta^f}{\partial x_i} = \frac{\partial^2}{\partial t^2}(\rho_{11}u_i + \rho_{12}U_i), \tag{4}$$

$$R\frac{\partial^2 U_j}{\partial x_i \partial x_j} + Q\frac{\partial^2 u_j}{\partial x_i \partial x_j} - R_{21}\frac{\partial \Theta^s}{\partial x_i} - R_{22}\frac{\partial \Theta^f}{\partial x_i} = \frac{\partial^2}{\partial t^2}(\rho_{12}u_i + \rho_{22}U_i), \tag{5}$$

(c) Heat Equations

$$K^s\frac{\partial^2 \Phi^s}{\partial x_i^2} = \frac{\partial^2}{\partial t^2}(F_{11}\Theta^s + F_{12}\Theta^f + T_0 R_{11}e_{ii} + T_0 R_{21}\epsilon), \tag{6}$$

$$K^f\frac{\partial^2 \Phi^f}{\partial x_i^2} = \frac{\partial^2}{\partial t^2}(F_{21}\Theta^s + F_{22}\Theta^f + T_0 R_{12}e_{ii} + T_0 R_{22}\epsilon), \tag{7}$$

where $R_{11}, R_{12}, R_{21}, R_{22},$ and J are mixed and thermal coefficients. ${C_E}^s, {C_E}^f$ are specific heats of phases at constant strain. u_i, U_i are displacements of the skeleton and fluid phases. K^s, K^f are characteristics of Green and Naghdi theory for solid and fluid phases, respectively. $\rho_{11} = \rho^s - \rho_{12}$ is mass coefficient of solid phase. $\rho_{22} = \rho^f - \rho_{12}$ is mass coefficient of fluid phase. ρ_{12} is dynamic coupling coefficient. $\rho^f = \beta\rho^{f*}$ is density of fluid phase per unit volume of the bulk. $\rho^s = (1-\beta)\rho^{s*}$ is density of solid phase per unit volume of the bulk. ρ^{f*}, ρ^{s*} are densities of the fluid and solid phases. β is porosity of material. $\lambda, \mu, R,$ and Q are poroelastic coefficients. $F_{11} = \rho^s {C_E}^s, F_{22} = \rho^f {C_E}^f, F_{12} = F_{21} = -JT_0, \Theta^s = T^s - T_0, (|\frac{\Theta^s}{T_0}| << 1), \Theta^f = T^f - T_0, (|\frac{\Theta^f}{T_0}| << 1),$ where in the reference state $T^s = T^f = T_0$. The conductive temperatures Φ^s, Φ^f satisfy the following relations

$$\Phi^s - \Theta^s = a^{*s}\frac{\partial^2 \Phi^s}{\partial x_i^2}, \quad \Phi^f - \Theta^f = a^{*f}\frac{\partial^2 \Phi^f}{\partial x_i^2}, \tag{8}$$

where a^{*s} and a^{*f} are two-temperature parameters of solid and fluid phases, respectively.

3 Velocity Equations

We consider a porothermoelastic solid half-space in $x-y$ plane, whose traction-free surface is along x-axis and positive y-axis is taken into the half-space. Using the following Helmholtz [70] decomposition, the displacement components of skeleton and fluid phases are

$$u_1 = \frac{\partial \phi^s}{\partial x} - \frac{\partial \psi^s}{\partial y}, \qquad u_2 = \frac{\partial \phi^s}{\partial y} + \frac{\partial \psi^s}{\partial x}, \tag{9}$$

$$U_1 = \frac{\partial \phi^f}{\partial x} - \frac{\partial \psi^f}{\partial y}, \qquad U_2 = \frac{\partial \phi^f}{\partial y} + \frac{\partial \psi^f}{\partial x}. \tag{10}$$

Using (9) and (10), Eqs. 4 to 8 are written in $x-y$ plane as

$$(\lambda + 2\mu)\nabla^2\phi^s + Q\nabla^2\phi^f - R_{11}\Theta^s - R_{12}\Theta^f = \frac{\partial^2}{\partial t^2}(\rho_{11}\phi^s + \rho_{12}\phi^f), \tag{11}$$

$$\mu\nabla^2\psi^s = \frac{\partial^2}{\partial t^2}(\rho_{11}\psi^s + \rho_{12}\psi^f), \tag{12}$$

$$R\nabla^2\phi^f + Q\nabla^2\phi^s - R_{21}\Theta^s - R_{22}\Theta^f = \frac{\partial^2}{\partial t^2}(\rho_{12}\phi^s + \rho_{22}\phi^f), \tag{13}$$

$$\frac{\partial^2}{\partial t^2}(\rho_{12}\psi^s + \rho_{22}\psi^f) = 0, \tag{14}$$

$$K^s\nabla^2\Phi^s = \frac{\partial^2}{\partial t^2}(F_{11}\Theta^s + F_{12}\Theta^f + T_0R_{11}\nabla^2\phi^s + T_0R_{21}\nabla^2\phi^f), \tag{15}$$

$$K^f\nabla^2\Phi^f = \frac{\partial^2}{\partial t^2}(F_{21}\Theta^s + F_{22}\Theta^f + T_0R_{12}\nabla^2\phi^s + T_0R_{22}\nabla^2\phi^f), \tag{16}$$

$$\Theta^s = (1 - a^{*s}\nabla^2)\Phi^s, \quad \Theta^f = (1 - a^{*f}\nabla^2)\Phi^f, \tag{17}$$

where $\nabla^2 = \dfrac{\partial^2}{\partial x^2} + \dfrac{\partial^2}{\partial y^2}$.

The solutions of the Eqs. 11 to 17 are now sought in the following form of harmonic traveling wave

$$\{\phi^s,\ \phi^f,\ \psi^s,\ \psi^f,\ \Phi^s,\ \Phi^f\} = \{\bar{\phi}^s,\ \bar{\phi}^f,\ \bar{\psi}^s,\ \bar{\psi}^f,\ \bar{\Phi}^s,\ \bar{\Phi}^f\}e^{\iota k(\sin\theta x + \cos\theta y - vt)}, \tag{18}$$

in which v is the complex phase speed, k is the wave number, $(\sin\theta, \cos\theta)$ denotes the projection of the wave normal onto $x-y$ plane. $\bar{\phi}^s$, $\bar{\phi}^f$, $\bar{\psi}^s$, $\bar{\psi}^f$, $\bar{\Phi}^s$, and $\bar{\Phi}^f$ are constants.

With the help of Eq. 18, Eqs. 11 to 17 lead to the following two velocity equations,

$$A(v^2)^4 + B(v^2)^3 + C(v^2)^2 + D(v^2) + E = 0, \tag{19}$$

$$v^2 = \frac{\rho_{22}\mu}{\rho_{11}\rho_{22} - {\rho_{12}}^2}, \tag{20}$$

where the expressions for A, B, C, D and E are given in Appendix 1. The Eq. 19 is solved numerically by Ferrari's method, which gives four complex values of v^2 or the complex phase velocities $v_j, (j = 1, 2, \ldots, 4)$ of four coupled longitudinal waves in generalized porothermoelasticity, which we may call as P_1, P_2, P_3 and P_4 waves. For a particular value of j, the complex phase velocity $v_j = v_R + iv_I$, defines the real phase velocity $V_j = \frac{{v_R}^2+{v_I}^2}{v_R}$ and the attenuation quality factor $Q_j^{-1} = -\frac{2v_I}{v_R}$ for the corresponding wave. We call real phase velocity V_j as phase velocity in the remaining analysis. The velocity equation (20) corresponds to the phase velocity V_5 of the shear wave. In particular case, if we put $K^s = K^f = 0, R_{11} = R_{12} = R_{21} = R_{22} = 0, a^{*s} = a^{*f} = 0$, Eq. 19 reduces to

$$({\rho_{11}\rho_{22} - {\rho_{12}}^2})\zeta^2 - \{(\lambda + 2\mu)\rho_{22} + R\rho_{11} - 2Q\rho_{12}\}\zeta + \{(\lambda + 2\mu)R - Q^2\} = 0, \tag{21}$$

which gives the same two roots as obtained by Hajra and Mukhopadhyay [9] for fast and slow P waves.

4 Reflection from Free Surface

A reflection phenomenon of incident longitudinal and shear waves is considered at a thermally insulated and stress-free surface of a Green–Naghdi type porothermoelastic solid half-space with two-temperature. Incident P_1 or SV waves gets reflected from thermally insulated and stress-free surface and five reflected waves P_1, P_2, P_3, P_4 and SV waves are obtained as shown in Fig. 1.

The relevant boundary conditions at the free surface $y = 0$ are

$$\sigma_{22} = 0, \quad \sigma_{12} = 0, \quad \sigma = 0, \quad \frac{\partial \Phi^s}{\partial y} = 0, \quad \frac{\partial \Phi^f}{\partial y} = 0, \tag{22}$$

where

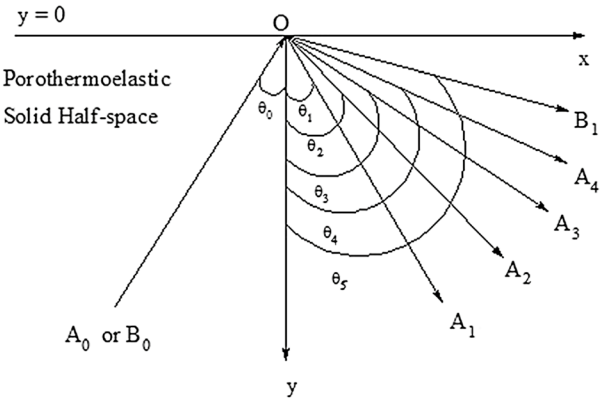

Fig. 1 Geometry showing directions of incident and reflected waves with normal to stress-free and thermally insulated surface

$$\sigma_{22} = \lambda\frac{\partial^2\phi^s}{\partial x^2} + (\lambda+2\mu)\frac{\partial^2\phi^s}{\partial y^2} + 2\mu\frac{\partial^2\psi^s}{\partial x\partial y} + Q\left(\frac{\partial^2\phi^f}{\partial x^2} + \frac{\partial^2\phi^f}{\partial y^2}\right) - R_{11}\left[\Phi^s - a^{*s}\left(\frac{\partial^2\Phi^s}{\partial x^2} + \frac{\partial^2\Phi^s}{\partial y^2}\right)\right] - R_{12}\left[\Phi^f - a^{*f}\left(\frac{\partial^2\Phi^f}{\partial x^2} + \frac{\partial^2\Phi^f}{\partial y^2}\right)\right],$$

$$\sigma_{12} = \mu\left(2\frac{\partial^2\phi^s}{\partial x\partial y} + \frac{\partial^2\psi^s}{\partial x^2} - \frac{\partial^2\psi^s}{\partial y^2}\right),$$

$$\sigma = R\left(\frac{\partial^2\phi^f}{\partial x^2} + \frac{\partial^2\phi^f}{\partial y^2}\right) + Q\left(\frac{\partial^2\phi^s}{\partial x^2} + \frac{\partial^2\phi^s}{\partial y^2}\right) - R_{21}\left[\Phi^s - a^{*s}\left(\frac{\partial^2\Phi^s}{\partial x^2} + \frac{\partial^2\Phi^s}{\partial y^2}\right)\right] - R_{22}\left[\Phi^f - a^{*f}\left(\frac{\partial^2\Phi^f}{\partial x^2} + \frac{\partial^2\Phi^f}{\partial y^2}\right)\right].$$

The appropriate potentials which satisfy the boundary conditions (22) are as

$$\phi^s = A_0 exp\{ik_1(\sin\theta_0 x - \cos\theta_0 y - V_1 t)\} + \sum_{i=1}^{4} A_i exp\{ik_i(\sin\theta_i x + \cos\theta_i y - V_i t)\}, \tag{23}$$

$$\phi^f = \eta_1 A_0 exp\{ik_1(\sin\theta_0 x - \cos\theta_0 y - V_1 t)\} + \sum_{i=1}^{4} \eta_i A_i exp\{ik_i(\sin\theta_i x + \cos\theta_i y - V_i t)\}, \tag{24}$$

$$\Phi^s = \zeta_1 A_0 exp\{ik_1(\sin\theta_0 x - \cos\theta_0 y - V_1 t)\} + \sum_{i=1}^{4} \zeta_i A_i exp\{ik_i(\sin\theta_i x + \cos\theta_i y - V_i t)\}, \tag{25}$$

$$\begin{aligned}\Phi^f =&\xi_1 A_0 exp\{ik_1(\sin\theta_0 x - \cos\theta_0 y - V_1 t)\}\\ &+ \sum_{i=1}^{4} \xi_i A_i exp\{ik_i(\sin\theta_i x + \cos\theta_i y - V_i t)\},\end{aligned} \tag{26}$$

$$\begin{aligned}\psi^s =&B_0 exp\{ik_5(\sin\theta_0 x - \cos\theta_0 y - V_5 t)\}\\ &+ B_1 exp\{ik_5(\sin\theta_5 x + \cos\theta_5 y - V_5 t)\},\end{aligned} \tag{27}$$

where the expressions of η_i, ζ_i and ξ_i (i = 1, 2,…, 4) are given in Appendix 2.

The potentials (23) to (27) satisfy the boundary conditions (22) if following relations (Snell's law) hold at $y = 0$,

$$\frac{\sin\theta_0}{V_1 or V_5} = \frac{\sin\theta_1}{V_1} = \frac{\sin\theta_2}{V_2} = \frac{\sin\theta_3}{V_3} = \frac{\sin\theta_4}{V_4} = \frac{\sin\theta_5}{V_5}, \tag{28}$$

$$k_1 V_1 = k_2 V_2 = k_3 V_3 = k_4 V_4 = k_5 V_5, \tag{29}$$

and, we obtain a non-homogenous system of five equations as

$$\sum_{j=1}^{5} a_{ij} Z_j = b_i, \quad (i = 1, 2, \ldots, 5) \tag{30}$$

where for $m = 1, 2, \ldots .5$,

$$a_{1m} = \left[\lambda + 2\mu\cos^2\theta_m + Q\eta_m + R_{11}(1 + a^{*s}k_m^2)\frac{\zeta_m}{k_m^2} + R_{12}(1 + a^{*f}k_m^2)\frac{\xi_m}{k_m^2}\right]\left(\frac{k_m}{k^*}\right)^2,$$

$$a_{15} = \mu\sin 2\theta_5\left(\frac{k_5}{k^*}\right)^2,$$

$$a_{2m} = -\sin 2\theta_m\left(\frac{k_m}{k^*}\right)^2, \quad a_{25} = \cos 2\theta_5\left(\frac{k_5}{k^*}\right)^2,$$

$$a_{3m} = [Q + R\eta_m + R_{21}(1 + a^{*s}k_m^2)\frac{\zeta_m}{k_m^2} + R_{22}(1 + a^{*f}k_m^2)\frac{\xi_m}{k_m^2}]\left(\frac{k_m}{k^*}\right)^2, \quad a_{35} = 0,$$

$$a_{4m} = \cos\theta_m(1 + a^{*s}k_m^2)\frac{\zeta_m}{k_m^2}\left(\frac{k_m}{k^*}\right)^3, \quad a_{45} = 0,$$

$$a_{5m} = \cos\theta_m(1 + a^{*f}k_m^2)\frac{\xi_m}{k_m^2}\left(\frac{k_m}{k^*}\right)^3, \quad a_{55} = 0,$$

and, for incident P_1 wave ($k^* = k_1$),

$$b_1 = -a_{11}, \quad b_2 = a_{21}, \quad b_3 = -a_{31}, \quad b_4 = a_{41}, \quad b_5 = a_{51},$$

$$Z_1 = \frac{A_1}{A_0}, \quad Z_2 = \frac{A_2}{A_0}, \quad Z_3 = \frac{A_3}{A_0} \quad Z_4 = \frac{A_4}{A_0} \quad Z_5 = \frac{B_1}{A_0},$$

and, for incident SV wave ($k^* = k_5$),

$$b_1 = a_{15}, \quad b_2 = -a_{25}, \quad b_3 = b_4 = b_5 = 0,$$
$$Z_1 = \frac{A_1}{B_0}, \quad Z_2 = \frac{A_2}{B_0}, \quad Z_3 = \frac{A_3}{B_0} \quad Z_4 = \frac{A_4}{B_0} \quad Z_5 = \frac{B_1}{B_0},$$

where Z_1, Z_2, Z_3, Z_4 and Z_5 are reflection coefficients (amplitude ratios) of the reflected P_1, P_2, P_3, P_4 and SV waves, respectively.

5 Energy Ratios

Following Achenbach [71], the rate of energy transmission per unit surface area is given by

$$P^* = \sigma_{22}\dot{u}_2 + \sigma_{12}\dot{u}_1 + \sigma\dot{U}_2. \tag{31}$$

Using Eq. 31, the expressions of energy ratios for all reflected waves are obtained as

Case (a): Incident P_1 waves

$$|E_j| = \frac{X_j}{X_0}\left(\frac{V_1}{V_j}\right)^3 Z_j^2, \ (j = 1, 2, \ldots, 4), \quad |E_5| = \frac{Y_1}{X_0}\left(\frac{V_1}{V_5}\right)^3 Z_5^2, \tag{32}$$

Case (b): Incident SV waves

$$|E_j| = \frac{X_j}{Y_0}\left(\frac{V_5}{V_j}\right)^3 Z_j^2, \ (j = 1, 2, \ldots, 4), \quad |E_5| = \frac{Y_1}{Y_0} Z_5^2, \tag{33}$$

where

$$X_j = \mu \sin\theta_j \ \sin 2\theta_j + \left[\lambda + 2\mu \cos^2\theta_j + Q\eta_j + R_{11}(1 + a^{*s}k_j^2)\frac{\zeta_j}{k_j^2} + R_{12}(1 + a^{*f}k_j^2)\frac{\xi_j}{k_j^2}\right] \cos\theta_j$$
$$+ \left[R\eta_j + Q + R_{21}(1 + a^{*s}k_j^2)\frac{\zeta_j}{k_j^2} + R_{22}(1 + a^{*f}k_j^2)\frac{\xi_j}{k_j^2}\right]\eta_j \cos\theta_j, \quad (j = 0, 1, 2, 3, 4),$$
$$Y_0 = \sin 2\theta_0 \ \sin\theta_0 + \chi \ \cos 2\theta_0 \ \cos\theta_0, \ Y_1 = \sin 2\theta_5 \ \sin\theta_5 + \chi \ \cos 2\theta_5 \ \cos\theta_5,$$
$$\chi = (\mu - \rho_{11}V_5^2)/\rho_{12}V_5^2.$$

In absence of thermal parameters, the relations (30) between reflection coefficients and energy ratio expressions (32) and (33) reduce to those obtained by Hajra and Mukhopadhyay [9]. Also, for $\beta = 0$ and $\beta = 1$, the above wave characteristics analysis (speeds, reflection coefficients and energy ratios) reduces to those for the cases of solid phase and fluid phase, respectively. In case of $\beta = 0$, there exist three reflected plane waves as P_1, P_3 and SV waves for incident P_1

or SV wave. For $\beta = 1$, there exist three reflected plane waves as P_2, P_4 and SV waves when P_2 or SV waves are incident.

6 Numerical Results and Discussion

For numerical computations, a program in Fortran software is developed and the following experimental values of physical parameters of kerosene-saturated sandstone are taken from Yew and Jogi [72]

$$
\begin{aligned}
Q &= 0.99663 \times 10^{11}\ \text{dyne} \cdot \text{cm}^{-2},\ R = 0.07435 \times 10^{11}\ \text{dyne} \cdot \text{cm}^{-2},\\
\lambda &= 0.44363 \times 10^{11}\ \text{dyne} \cdot \text{cm}^{-2},\ \mu = 0.2765 \times 10^{11}\ \text{dyne} \cdot \text{cm}^{-2},\\
{\rho_f}^* &= 0.82\ \text{g} \cdot \text{cm}^{-3},\ \ {\rho_s}^* = 2.6\ \text{g} \cdot\ \text{cm}^{-3},\ \ \rho_{11} = 0.002137\ \text{g} \cdot\ \text{cm}^{-3},\\
K^s &= 0.4\ \text{cal} \cdot \text{cm}^{-1} \cdot \text{s}^{-1} \cdot {}^\circ\text{C}^{-1},\ \ K^f = 0.3\ \text{cal} \cdot \text{cm}^{-1} \cdot \text{s}^{-1} \cdot{}^\circ\ \text{C}^{-1},\\
{C_E}^s &= 2.1\ \text{cal} \cdot \text{g}^{-1} \cdot{}^\circ\ \text{C}^{-1},\ \ {C_E}^f = 1.9\ \text{cal} \cdot \text{g}^{-1} \cdot{}^\circ\ \text{C}^{-1},\ \ T_0 = 27\,{}^\circ\text{C},\\
\alpha^s &= 0.01\ \text{cm}^3 \cdot \text{g}^{-1},\ \alpha^f = 0.02\ \text{cm}^3 \cdot \text{g}^{-1},\ \alpha^{sf} = 0.03\ \text{cm}^3 \cdot \text{g}^{-1},\\
\alpha^{fs} &= 0.04\ \text{cm}^3 \cdot \text{g}^{-1},\ \ {\tau_0}^s = {\tau_0}^f = 0.005\ \text{s},\ \ \omega = 2\ \text{Hz}.
\end{aligned}
$$

The ratio of volumes of pore space to bulk space in a rock is called porosity. The porosity in most rocks lies in the range between less than 0.01 and 0.5. For present illustrations, the value of porosity is taken in the range between 0.01 and 0.5.

For the incidence of P_1 wave, the energy ratios of reflected waves are computed using Eqs. 30, 32 and 33. The energy ratios of reflected P_1, P_2, P_3, P_3 and SV waves are shown graphically in Figs. 2, 3, 4, 5, 6, 7, 8, 9, 10, 11 against the angle of incidence $\theta_0(1^\circ - 90^\circ)$ for different sets of two-temperature parameters with porosity $\beta = 0.4$. In these figures, five sets, I $(a^{*s} = 0, a^{*f} = 0)$; II $(a^{*s} = 0.4, a^{*f} = 0)$; III $(a^{*s} = 0.8, a^{*f} = 0)$; IV $(a^{*s} = 0, a^{*f} = 0.4)$ and V $(a^{*s} = 0, a^{*f} = 0.8)$, of two-temperature parameters are considered. In Figs. 2 and 3, the energy ratio of

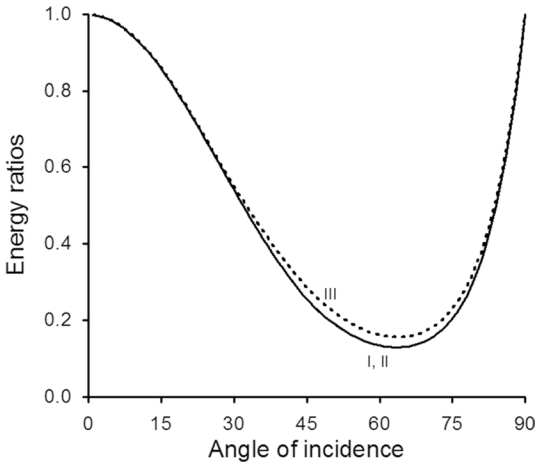

Fig. 2 Effect of two-temperature parameter a^{*s} on energy ratios of reflected P_1 wave for different sets of two-temperature parameters when porosity $\beta = 0.4$

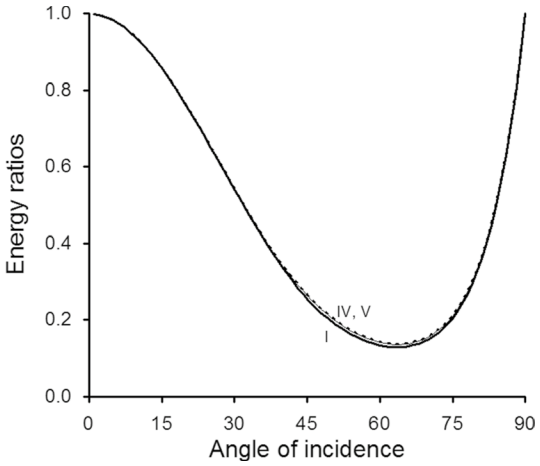

Fig. 3 Effect of two-temperature parameter a^{*f} on energy ratios of reflected P_1 wave for different sets of two-temperature parameters when porosity $\beta = 0.4$

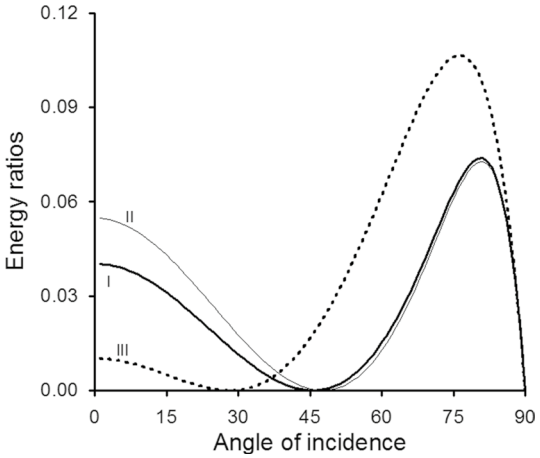

Fig. 4 Effect of two-temperature parameter a^{*s} on energy ratios of reflected P_2 wave for different sets of two-temperature parameters when porosity $\beta = 0.4$

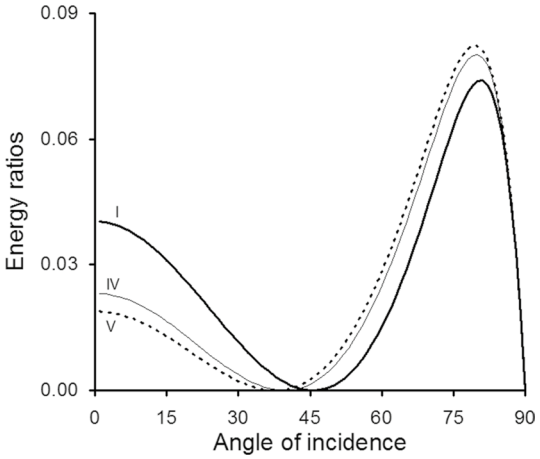

Fig. 5 Effect of two-temperature parameter a^{*f} on energy ratios of reflected P_2 wave for different sets of two-temperature parameters when porosity $\beta = 0.4$

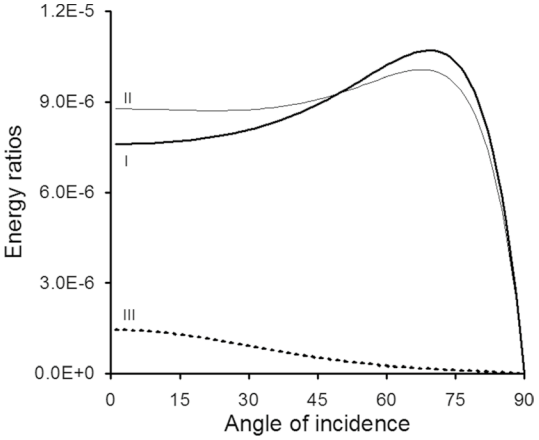

Fig. 6 Effect of two-temperature parameter a^{*s} on energy ratios of reflected P_3 wave for different sets of two-temperature parameters when porosity $\beta = 0.4$

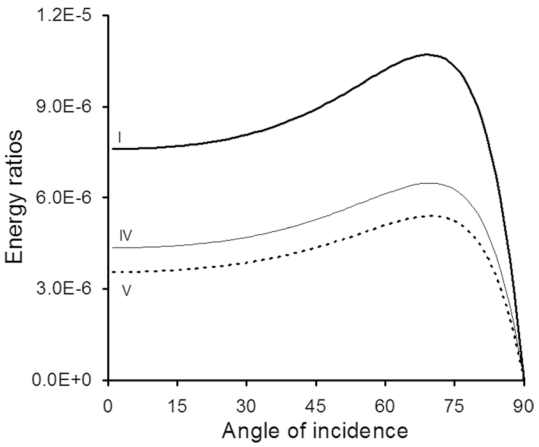

Fig. 7 Effect of two-temperature parameter a^{*f} on energy ratios of reflected P_3 wave for different sets of two-temperature parameters when porosity $\beta = 0.4$

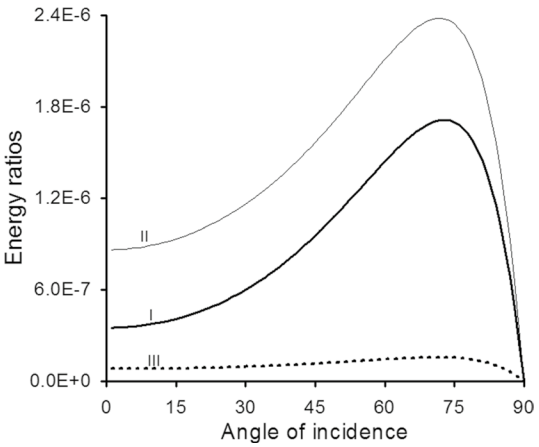

Fig. 8 Effect of two-temperature parameter a^{*s} on energy ratios of reflected P_4 wave for different sets of two-temperature parameters when porosity $\beta = 0.4$

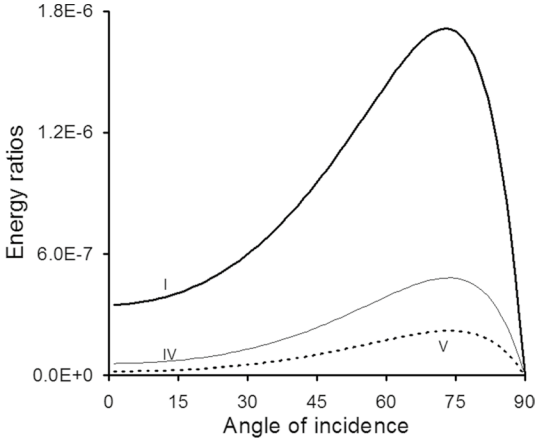

Fig. 9 Effect of two-temperature parameter a^{*f} on energy ratios of reflected P_4 wave for different sets of two-temperature parameters when porosity $\beta = 0.4$

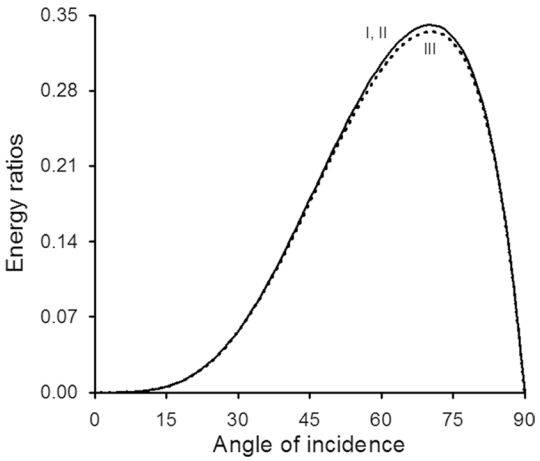

Fig. 10 Effect of two-temperature parameter a^{*s} on energy ratios of reflected SV wave for different sets of two-temperature parameters when porosity $\beta = 0.4$

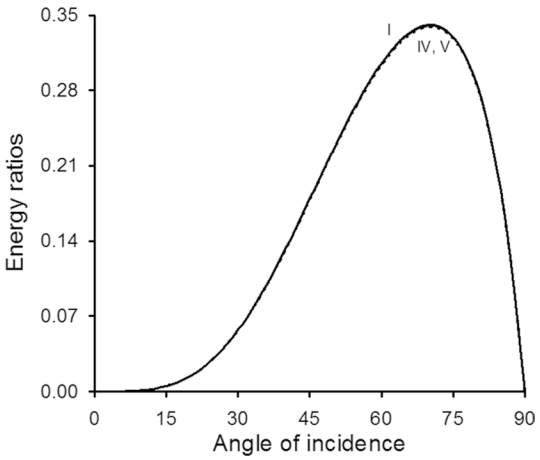

Fig. 11 Effect of two-temperature parameter a^{*f} on energy ratios of reflected SV wave for different sets of two-temperature parameters when porosity $\beta = 0.4$

reflected P_1 wave for set I ($a^{*s} = 0, a^{*f} = 0$) is 0.98366 at $\theta_0 = 1°$ and decreases monotonically with increasing angle of incidence and attains a minimum value 0.12824 at $\theta_0 = 64°$. Thereafter, it increases monotonically to its maximum value at $\theta_0 = 90°$ (grazing incidence). In Figs. 4 and 5, the energy ratio of reflected P_2 wave for set I is 0.04024 at $\theta_0 = 1°$ and it decreases monotonically to its minimum value 0.14258e-04 at $\theta_0 = 46°$. Beyond $\theta_0 = 46°$, it increases sharply to its maximum value 0.0739 at $\theta_0 = 81°$ and then decreases monotonically. In Figs. 6 and 7, the energy ratio of reflected P_3 wave for set I is 0.75995e-05 at $\theta_0 = 1°$ and it increases monotonically to its maximum value 0.10694e-04 at $\theta_0 = 69°$. Thereafter, it decreases sharply to its minimum value at $\theta_0 = 90°$. In Figs. 8 and 9, the energy ratio of reflected P_4 wave for set I is 0.34919e-06 at $\theta_0 = 1°$ and it increases monotonically to its maximum value 0.17133e-05 at $\theta_0 = 73°$. Thereafter, the energy ratio of reflected P_4 wave decreases very sharply to its minimum value at grazing incidence. In Figs. 10 and 11, the energy ratio of reflected SV wave is 0.39505e-05 at $\theta_0 = 1°$ and it increases monotonically and sharply to its maximum value 0.34095 at $\theta_0 = 70°$. Thereafter, it decreases sharply to its minimum value at grazing incidence. For other sets (II, III, IV and V) of two-temperature parameters, the energy ratio variations of all reflected waves are similar to set I. On comparing variations for set I with those of sets II and III in Figs. 2, 4, 6, 8 and 10, the effect of two-temperature parameter a^{*s} is observed on reflected longitudinal and shear waves. Also, on comparing variations for set I with those for sets IV and V in Figs. 3, 5, 7, 9 and 11, the effect of two-temperature parameter a^{*f} is observed on reflected longitudinal and shear waves.

The energy ratios of reflected P_1, P_2, P_3, P_3 and SV waves are also graphically illustrated in Figs. 12 , 13, 14, 15, and 16 against the angle of incidence θ_0 ($1° - 90°$) for different values of porosity β, when $a^{*s} = 0.3,$ and $a^{*f} = 0.3$. The thick solid, thin solid and dashed curves in these figures correspond to $\beta = 0.3, 0.4$ and 0.5, respectively. The effect of porosity on energy ratios of reflected waves is observed at every incident angle ranging between $\theta_0 = 1°$ and $\theta_0 = 89°$. However, no effect of porosity is observed at grazing incidence ($\theta_0 = 90°$).

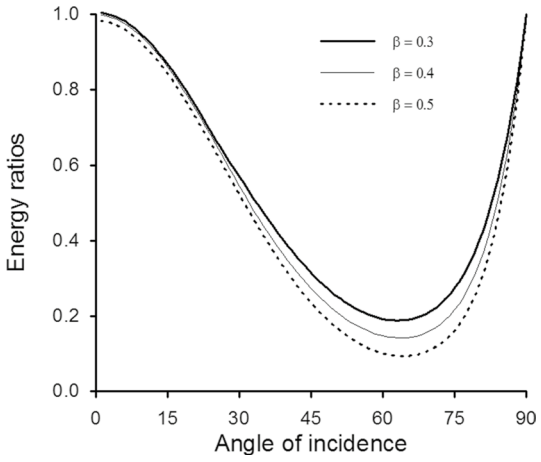

Fig. 12 Effect of porosity on energy ratios of reflected P_1 wave when $a^{*s} = 0.3, a^{*f} = 0.3$

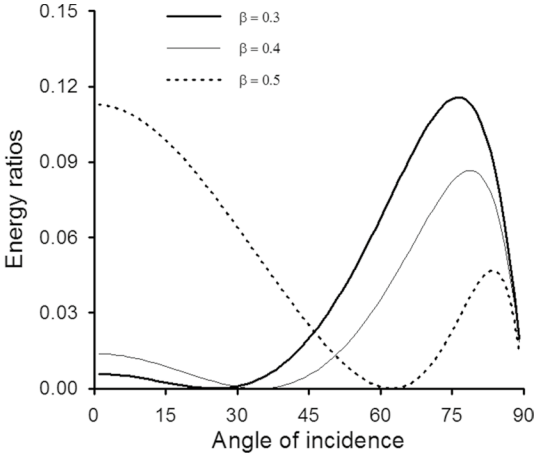

Fig. 13 Effect of porosity on energy ratios of reflected P_2 wave when $a^{*s} = 0.3, a^{*f} = 0.3$

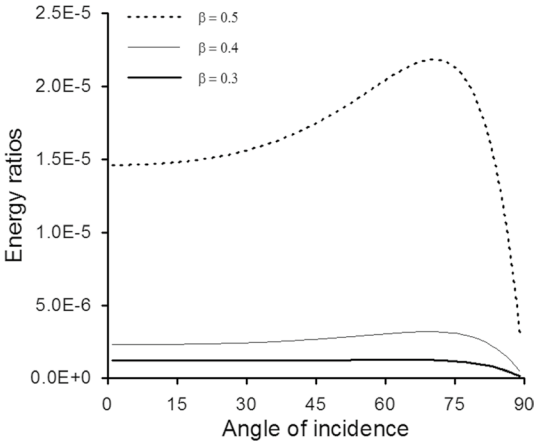

Fig. 14 Effect of porosity on energy ratios of reflected P_3 wave when $a^{*s} = 0.3, a^{*f} = 0.3$

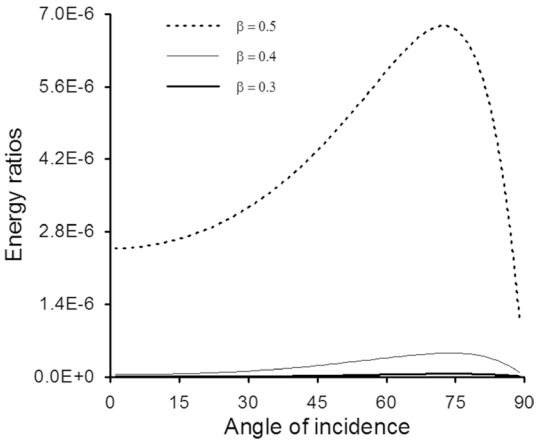

Fig. 15 Effect of porosity on energy ratios of reflected P_4 wave when $a^{*s} = 0.3, a^{*f} = 0.3$

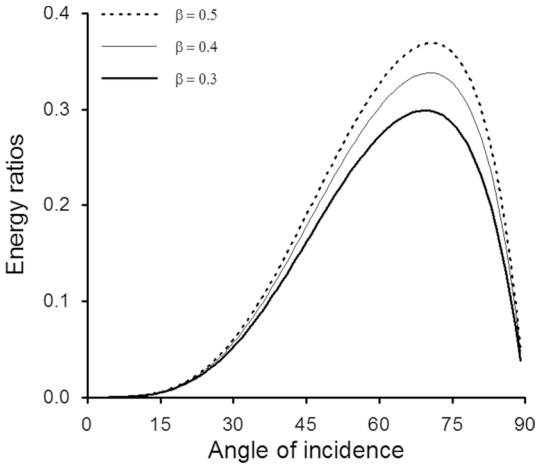

Fig. 16 Effect of porosity on energy ratios of reflected *SV* wave when $a^{*s} = 0.3, a^{*f} = 0.3$

7 Conclusions

The Green and Nagdhi theory of thermoelasticity is applied for formulating the governing equations of two-temperature porothermoelasticity without energy dissipation. The governing equations are specialized for a plane and are solved for plane wave solutions. It is found that there exist one shear and four coupled longitudinal waves in a half-space model. A problem on reflection of plane waves is studied at a thermally insulated and traction-free surface. For incident longitudinal or shear wave, the relations between reflection coefficients and the expressions of energy ratios for reflected waves are obtained analytically. In case of incident P_1 wave, the energy ratios of all reflected waves are computed and graphically illustrated for different sets of two-temperature parameters and for different values of porosity. The energy ratios of reflected waves are affected due to change in values of two-temperature parameters and porosity. However, the effects of two-temperature parameters and porosity on energy ratios of reflected P_1 and *SV* waves are observed less as compared to other reflected longitudinal waves. In absence of thermal parameters, the present theoretical expressions and numerical results agree with those obtained by Hajra and Mukhopadhyay [9]. In absence of thermal effects, the reflected P_3 and P_4 waves do not exist and P_1 and P_2 waves correspond to fast-*P* and slow-*P* waves, respectively. For illustrations of numerical results, a model of kerosene-saturated sandstone is taken with porosity lying in the range between 0.01 and 0.5. The numerical results are obtained in terms of energy ratios of reflected waves. The sum of energy ratios of all reflected waves is found less than or equal to one at each angle of incidence. It is also observed that the P_2 and P_4 waves will not appear for porosity $\beta = 0$. Similarly for porosity $\beta = 1$, the P_1 and P_3 waves will not exist. These above facts may be helpful for validating the present model. Such theoretical investigations are expected to be useful for detecting and studying the porous layers saturated with groundwater or oil.

Acknowledgements Author (Baljeet Singh) acknowledges University Grants Commission, New Delhi for granting a Major Project (MRP-MAJOR-MATH-2013-2149).

Data and Resources Section The data used in computations are taken from published source (Yew and Jogi, 1976) cited in the reference list.

Compliance with Ethical Standards

Conflict of interest The author declares that he has no conflict of interest.

Appendices

Appendix 1

The expressions for A, B, C, D and E have been obtained as

$$
\begin{aligned}
A &= (\rho_{11}\rho_{22} - \rho_{12}^2)(F_{11}F_{22} - F_{12}F_{21}),\\
B &= (F_{12}F_{21} - F_{11}F_{22})[\rho_{22}(\lambda + 2\mu) + \rho_{11}R - 2\rho_{12}Q]\\
&\quad + (K^{*s}F_{22} + K^{*f}F_{11})(\rho_{12}^2 - \rho_{11}\rho_{22})\\
&\quad + T_0[F_{11}(2\rho_{12}R_{12}R_{22} - \rho_{11}R_{22}^2 - \rho_{22}R_{12}^2) + F_{22}(2\rho_{12}R_{11}R_{21} - \rho_{22}R_{11}^2 - \rho_{11}R_{21}^2)\\
&\quad + (F_{12} + F_{21})(\rho_{22}R_{11}R_{22} + \rho_{11}R_{21}R_{22} - \rho_{12}R_{12}R_{21} - \rho_{12}R_{11}R_{22})],\\
C &= (F_{11}F_{22} - F_{12}F_{21})[(\lambda + 2\mu)R - Q^2](K^{*s}F_{22} + K^{*f}F_{11})[(\lambda + 2\mu)\rho_{22}\\
&\quad + \rho_{11}R - 2\rho_{12}Q]\\
&\quad + K^{*s}T_0[\rho_{11}R_{22}^2 + \rho_{22}R_{12}^2 - 2\rho_{12}R_{12}R_{22}] + K^{*f}T_0[\rho_{11}R_{21}^2 + \rho_{22}R_{11}^2 - 2\rho_{12}R_{11}R_{21}]\\
&\quad + K^{*s}K^{*f}(\rho_{11}\rho_{22} - {\rho_{12}}^2) + T_0^2(R_{11}^2R_{22}^2 + R_{12}^2R_{21}^2 - 2R_{11}R_{21}R_{12}R_{22})\\
&\quad + T_0[(\lambda + 2\mu)\{R_{21}^2F_{22} + R_{22}^2F_{11} - R_{21}R_{22}(F_{12} + F_{21})\}\\
&\quad + Q\{(F_{12} + F_{21})(R_{11}R_{22} + R_{12}R_{21}) - 2R_{11}R_{21}F_{22} - 2R_{12}R_{22}F_{11}\}\\
&\quad + R\{R_{11}^2F_{22} + R_{12}^2F_{11} - R_{11}R_{12}(F_{12} + F_{21})\}],\\
D &= -K^{*s}K^{*f}[\rho_{22}(\lambda + 2\mu) + \rho_{11}R - 2\rho_{12}Q] + K^{*s}[Q^2F_{22} + 2QR_{12}R_{22} - RR_{12}^2\\
&\quad - (\lambda + 2\mu)(T_0R_{22}^2 + RF_{22})] + K^{*f}[Q^2F_{11} + 2QR_{11}R_{21} - RR_{11}^2\\
&\quad - (\lambda + 2\mu)(T_0R_{21}^2 + RF_{11})],\\
E &= K^{*s}K^{*f}[R(\lambda + 2\mu) - Q^2],
\end{aligned}
$$

where $K^{*s} = \frac{K^s}{1+a^{*s}k^2}$ and $K^{*s} = \frac{K^f}{1+a^{*f}k^2}$.

Appendix 2

The expressions for η_i, ζ_i and ξ_i (i = 1, 2,…, 4) are derived as

$$
\eta_i = -\left[\frac{\Delta T_0R_{11}V_i^2 + (K^{*s} - V_i^2F_{11})(R_{22}W_1 - R_{12}W_2) + F_{12}V_i^2(R_{21}W_1 - R_{11}W_2)}{\Delta T_0R_{21}V_i^2 + (K^{*s} - V_i^2F_{11})(R_{22}W_2 - R_{12}W_3) + F_{12}V_i^2(R_{21}W_2 - R_{11}W_3)}\right], \tag{34}
$$

$$\zeta_i = \frac{k_i^2}{(1 + a^{*s} k_i^2)} \left[\frac{R_{22} W_1 - R_{12} W_2 + \eta_i (R_{22} W_2 - R_{12} W_3)}{\Delta} \right], \tag{35}$$

$$\xi_i = - \frac{k_i^2}{(1 + a^{*f} k_i^2)} \left[\frac{R_{21} W_1 - R_{11} W_2 + \eta_i (R_{21} W_2 - R_{11} W_3)}{\Delta} \right], \tag{36}$$

where

$$\Delta = R_{12} R_{21} - R_{11} R_{22},\ W_1 = (\lambda + 2\mu) - \rho_{11} V_i^2,\ W_2 = Q - \rho_{12} V_i^2,\ W_3 = R - \rho_{22} V_i^2.$$

References

1. M.A. Biot, J. Appl. Mech. **23**, 91 (1956)
2. M.A. Biot, J. Acoust. Soc. Am. **28**, 168 (1956)
3. M.A. Biot, J. Appl. Phys. **33**, 1482 (1962)
4. H. Deresiewicz, J.T. Rice, Bull. Seismol. Soc. Am. **52**, 595 (1962)
5. C. Pecker, H. Deresiewicz, Acta Mech. **16**, 45 (1973)
6. J.G. Berryman, Appl. Phys. Lett. **37**, 382 (1980)
7. J.G. Berryman, Geophysics **70**, N1 (2005)
8. T.J. Plona, Appl. Phys. Lett. **36**, 259 (1980)
9. S. Hajra, A. Mukhopadhyay, Bull. Seismol. Soc. Am. **72**, 1509 (1982)
10. M.D. Sharma, M.L. Gogna, J. Acoust. Soc. Am. **90**, 1068 (1991)
11. D.L. Johnson, T.J. Plona, H. Kojima, J. Appl. Phys. **76**, 115 (1994)
12. J.M. Carcione, J. Acoust. Soc. Am. **99**, 2655 (1996)
13. O. Kelder, D.M.J. Smeulders, Geophysics **62**, 1794 (1997)
14. N.K. Nakagawa, K. Soga, J.K. Mitchell, Geotechnique **47**, 133 (1997)
15. A. Gajo, A. Fedel, L. Mongiovi, Geotechnique **47**, 993 (1997)
16. N. Khalili, M. Yazdchi, S. Valliappan, Soil Dyn. Eq. Eng. **18**, 533 (1999)
17. M. Tajuddin, S.J. Hussaini, J. Appl. Geophys. **58**, 59 (2005)
18. B. Albers, K. Wilmanski, Arch. Mech. **58**, 313 (2006)
19. J.-T. Wang, F. Jin, C.-H. Zhang, Ocean Eng. **63**, 8 (2013)
20. M.D. Sharma, J. Earth Syst. Sci. **116**, 357 (2007)
21. Y. Li, Z.-W. Cui, Y.-J. Zhang, K.-X. Wang, Rock Soil Mech. **28**, 1595 (2007)
22. F.I. Zyserman, J.E. Santos, Compt. Methods Appl. Mech. Eng. **196**, 4644 (2007)
23. S. Nakagawa, M.A. Schoenberg, J. Acoust. Soc. Am. **122**, 831 (2007)
24. W.-C. Lo, Adv. Water Res. **31**, 1399 (2008)
25. C.-L. Yeh, W.-C. Lo, C.-D. Jan, C.-C. Yang, J. Hydrol. **395**, 91 (2010)
26. M.D. Sharma, IMA, J. Appl. Math. **78**, 59 (2013)
27. M.D. Sharma, J. Porous Media **21**, 35 (2018)
28. D. Wang, H.-L. Zhang, X.-M. Wang, Chin. J. Geophys. **49**, 524 (2006)
29. R. Chattaraj, L. Samal, Meccanica **51**, 2215 (2016)
30. E. Wang, J.M. Carcione, J. Ba, Y. Liu, Surv. Geophys. **41**, 283 (2019)
31. S. Hoseinzadeh, P.S. Heyns, A.J. Chamkha, A. Shirkhani, J. Therm. Anal. Calorim. (2019). https://doi.org/10.1007/s10973-019-08203-x
32. S. Hoseinzadeh, A. Moafi, A. Shirkhani, A.J. Chamkha, J. Thermophys. Heat Transf. (2019). https://doi.org/10.2514/1.t5583
33. S. Hoseinzadeh, R. Ghasemiasl, D. Havaei, A.J. Chamkha, J. Mol. **271**, 655 (2019)
34. M.H. Ghasemi, S. Hoseinzadeh, P.S. Heyns, D.N. Wilke, Comput. Model. Eng. Sci. **122**, 399 (2020)
35. M.A. Biot, J. Appl. Phys. **27**, 240 (1956)
36. R.L. Schiffman, in Environmental and Geophysical Heat Transfer, vol. 99 (ASME, New York, 1971), pp. 78–84

37. R.M. Bowen, Acta Mech. **46**, 189 (1983)
38. D. McTigue, J. Geophys. Res. **91**, 9533 (1986)
39. M. Kurashige, Int. J. Solids Struct. **25**, 1039 (1989)
40. J. Bear, S. Sorek, G. Ben-Dor, G. Mazor, Fluid Dyn. Res. **9**, 155 (1992)
41. S. Sorek, J. Bear, G. Ben-Dor, G. Mazor, Transport Porous Med. **9**, 3 (1992)
42. Y. Zhou, R.K.N.D. Rajapakse, J. Graham, Int. J. Solids Struct. **35**, 4659 (1998)
43. A. Ghassemi, A. Diek, J. Petrol. Sci. Eng. **34**, 123 (2002)
44. Y. Abousleiman, S. Ekbote, J. Appl. Mech. **72**, 102 (2005)
45. H.M. Youssef, Int. J. Rock Mech. Min. Sci. **44**, 222 (2007)
46. M.D. Sharma, J. Earth Syst. Sci. **117**, 951 (2008)
47. B. Singh, Bull. Seismol. Soc. Am. **101**, 756 (2011)
48. B. Singh, J. Porous Media. **16**, 945–957 (2013)
49. T. Haibing, L. Ganbin, X. Kanghe, Z. Rongyue, D. Yuebao, Transport Porous Med. **103**, 47 (2014)
50. W. Wei, R.Y. Zheng, G.B. Liu, H.B. Tao, Transport Porous Med. **395**, 1 (2016)
51. B. Singh, in Poromechanics VI (ASCE, 2017), pp. 1706–1713
52. M.D. Sharma, Waves Random Complex Media **28**, 570 (2018)
53. J.M. Carcione, F. Cavallini, E. Wang, J. Ba, L.-Y. Fu, J. Geophys. Res. Solid Earth **124**, 8147 (2019)
54. F. Zhou, H. Liu, S. Li, J. Therm. Stresses **42**, 1256 (2019)
55. F. Zhou, R. Zhang, H. Liu, G. Yue, J. Therm. Stresses (2020). https://doi.org/10.1080/01495739.2019.1711478
56. P.J. Chen, M.E. Gurtin, Z. Angew, Math. Phys. **19**, 614 (1968)
57. P.J. Chen, M.E. Gurtin, W.O. Williams, Z. Angew, Math. Phys. **19**, 969 (1968)
58. P.J. Chen, M.E. Gurtin, W.O. Williams, Z. Angew, Math. Phys. **20**, 107 (1969)
59. W.E. Warren, P.J. Chen, Acta Mech. **16**, 21 (1973)
60. P. Puri, P.M. Jordan, Int. J. Eng. Sci. **44**, 1113 (2006)
61. H.M. Youssef, J. Appl. Math. **71**, 383 (2006)
62. H.M. Youssef, J. Therm. Stresses **34**, 138 (2011)
63. H. Lord, Y. Shulman, J. Mech. Phys. Solids **15**, 299 (1967)
64. A.E. Green, P.M. Naghdi, J. Elast. **31**, 189 (1993)
65. R. Kumar, S. Mukhopadhyay, Int. J. Eng. Sci. **48**, 128 (2010)
66. B. Singh, K. Bala, J. Mech. Mater. Struct. **7**, 183 (2012)
67. R. Bijarnia, B. Singh, Int. J. Appl. Mech. Eng. **21**, 285 (2016)
68. M.I.A. Othman, S. Said, M. Marin, Int. J. Numer. Methods Heat Fluid Flows **29**, 4788 (2019)
69. C. D'Apice, V. Zampoli, S. Chiriţă, J. Elast. (2020) https://doi.org/10.1007/s10659-020-09770-z
70. H. Helmholtz, J. Reine Angew Math. **55**, 25 (1858)
71. J.D. Achenbach, *Wave Propagation in Elastic Solids* (Elsevier, North Holland, 1973)
72. C.H. Yew, P.N. Jogi, J. Acoust. Soc. Am. **60**, 2 (1976)